Electronic excitation by short X-ray pulses: From quantum beats to wave packet revivals

Paula Rivière,[1,2] Shahid Iqbal,[1] and Jan M Rost[1,3]

[1] *Max-Planck Institute for the Physics of Complex Systems Nöthnitzer Str. 38, 01187 Dresden, Germany.*

[2] *Departamento de Química, Universidad Autónoma de Madrid, 28049 Madrid, Spain.*

[3] *Advanced Study Group at the Center for Free Electron Laser Science, DESY, Hamburg, Germany*

(Dated: September 27, 2011)

We propose a simple way to determine the periodicities of wave packets in quantum systems directly from the energy differences of the states involved. The resulting classical periods and revival times are more accurate than those obtained with the traditional expansion of the energies about the central quantum number $\overline{n}$, especially when $\overline{n}$ is low. The latter type of wave packet motion occurs upon excitation of highly charged ions with short XUV or X-ray pulses. Moreover, we formulate the wave packet dynamics in such a form that it directly reveals the origin of phase shifts in the maxima of the autocorrelation function. This phenomenon, so far poorly understood since it is not prominent in the high $\overline{n}$ regime, becomes a dominant feature in low $\overline{n}$ wave packet dynamics.

PACS numbers: 32.80.Aa, 32.80.Ee, 42.50.Md

I. INTRODUCTION

A wave packet (WP) comprising many energy eigenstates of a system spreads during its time evolution, only to reverse the spreading and reshape after a certain time called the revival time. Originally formulated in the context of highly excited electrons in atoms [1] following the first observation of wave packet collapse and revival [2], the phenomenon has been identified in a large variety of physical systems, such as in Gaussian WPs in quantum boxes [3], the evolution of rovibrational nuclear WPs [4, 5] (for a review see [6]), even at an attosecond time scale [7], revivals in a coherent photon field [8], or recently, the propagation of WPs in graphene under magnetic fields [9].

Quantum revivals have also been widely studied over the years in a more mathematical context, with emphasis on obtaining accurate analytical expressions [10, 11], for a review see [12].

The multiple interferences of the wave packet components lead also to the so-called fractional revivals at divisors of the revival time, which have been predicted [13, 14] and observed in Rydberg wave packets [15] or photon bouncing balls [16]. Fractional revivals can retrieve information about the system even if it decays before the first revival [17]. They can be used for mapping the quantum phase of a molecular nuclear wave-packet in two-dimensional spectroscopy [18], or even to factorize prime numbers [19]. It has also been shown that information entropy in position and momentum spaces can reveal the existence of fractional revivals [20].

The study of quantum revivals in atoms has traditionally focused on the excitation of Rydberg WPs. The latter contain typically of the order of 10 highly excited states when they are centered on a principal quantum number $30 < \overline{n} < 85$ and excited by laser pulses with a duration of a few picoseconds [1]. Under these circumstances the relative difference between the energies of the states is small, and the standard approach of representing the energies of the contributing states by Taylor expansion about the central energy $E_{\overline{n}}$ provides good results.

However, new FEL or high harmonic-based light sources are able to deliver short pulses of 100 atomic units (2.4 fs) duration and less in the VUV to X-ray regime [21]. In particular the X-ray pulses will typically lead to a multi-electron wave packet of the valence shell of an atom by inner shell ionization. In order for the photo electron to form a bound wave packet while simultaneously the core electrons remain in their ground state, such wave packets must be generated in highly charged ions, as produced, e.g., in state-of-the-art electron-cyclotron ion sources (ECR) [22] or EBITs [23]. The high ionic charge implies large electronic energy spacings so that only a few levels contribute to the wave packet, despite the large energy width due to the short pulse duration. Hence, the dynamics lays in between quantum beats of a few well defined energy levels [24] and the traditional regime of Rydberg wave packets as discussed before.

A good estimate of the dynamical range of a system, which goes from quantum beats to wave packet revivals, is the number of states in the WP, k. One can estimate this number by relating the energy spread of the laser pulse to the energy spread in the excited atom, which for a WP centered in state $\overline{n}$ is $\Delta E \simeq k\, dE_n/dn|_{\overline{n}}$. An electric field of Gaussian shape $f(t) = f_0 \exp^{-2\ln 2 t^2/T^2}$, where T is the FWHM of the pulse and f_0 its amplitude, will populate a wave packet with amplitude

$$F_n = f_0 \exp^{-(E_n - E_{\overline{n}})^2 T^2/(8\log 2)} \tag{1}$$

for each energy level E_n. Including all those states with probability $\geq c$ implies an energy spread of $\Delta E = C/T$, where $C = 4(-\ln 2 \ln c)^{1/2}$. For a hydrogenic ion of charge Z and spectrum $E_n = -Z^2/(2n^2)$, equalling both

TABLE I: Number of states k contributing to a wave packet with up to an amplitude weight of $c = 10^{-2}$ when excited to a central state $\overline{n}$ by a pulse of duration T (FWHM). We assume an hydrogenic ion with energy spectrum $E_n = -Z^2/(2n^2)$. Parameters given are used in the figures of this paper as indicated.

k	Z	$\overline{n}$	T [fs]	Figs.
13	1	85	8000	1
8	1	45	2000	4,5
4	8	14	2	4,5
4	12	7	0.1	6
5	8	9	0.4	8

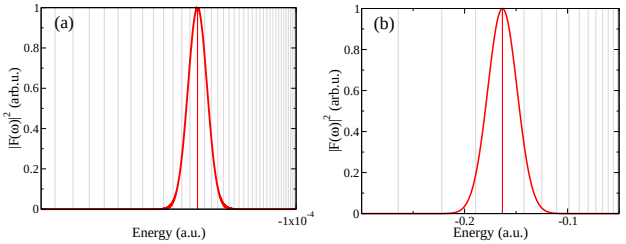

FIG. 1: (Color online) Field intensities in the frequency regime, $|F(\omega)|^2$, and energy levels for two regimes: (a) high $\overline{n}$, long pulses, for the particular case of $Z = 1$, $\overline{n} = 45$, FWHM=2 ps, (b) low $\overline{n}$, short pulses, for the case of $Z = 8$, $\overline{n} = 14$, FWHM=2 fs. The red vertical lines correspond to $\overline{n}$ in each case. For the number of energy levels participating in the wave packet with an amplitude of more than 10^{-2}, see table 1.

values of ΔE gives

$$k = C\overline{n}^3/(Z^2T). \tag{2}$$

A few quantitative examples of the number of states k as a function of $\overline{n}$ and T for different atomic numbers is shown in Table 1. Two cases of low and high $\overline{n}$ are shown in Fig. 1.

Our goal is to treat the low $\overline{n}$ regime of electron excitation from the perspective of wave packet revivals. However, due to the large energy spacing the standard description of the WPs with a harmonic approximation about $E_{\overline{n}}$ becomes rather inaccurate. In the following we will show that one can replace the derivatives of the energies by exact differences of energy levels to obtain a description which is valid in the new regime of short, high frequency pulses. This approach is conceptually very simple and it is universally valid, also in the traditional Rydberg regime. We can derive accurate values for the revival times in all situations. Moreover, the origin of the shift in the position of the maxima around the revival time, previously noticed [13, 25] but not well described, emerges naturally.

The structure of the paper is as follows: in section II, a form of the autocorrelation function is derived which allows one to explicitly read off the relevant periods. We also derive and explain why for the low excitation regime finite energy differences should be used to define these periods instead of energy derivatives. The periods, classical, revival and fractional revival times, as well as a feature which is important for low excitation wave packets, namely the time where the extrema flip their sign, are explained in section III with examples from the high and intermediate excitation domain. Section IV points out the characteristic features of low excitation wave packets ending with a hydrogenic ion excited by a 100 attosecond X-ray (1.92 keV) pulse. Finally, for multi-electron atoms, the effect of the quantum defect is discussed in V, and conclusions are drawn in VI.

II. AUTOCORRELATION FUNCTION

Without loss of generality but to be somewhat specific we consider a system which absorbs one photon from a laser pulse of length T in a transition from an initial state $|\alpha\rangle$ to a final state $|\overline{n}\rangle$ which, for simplicity, we assume to be an eigenstate of the system. Due to the finite length of the pulse, this process creates a wave packet which can be expressed in first order perturbation theory after the pulse as

$$|\Psi(t)\rangle \;=\; i\sum_n |n\rangle \exp[-iE_nt]M_{\alpha n}F_n, \tag{3}$$

where F_n are the amplitudes defined in Eq. (1). The dipole matrix elements $M_{\alpha n} = \langle n|z|\Psi_\alpha(0)\rangle$ give the strength of photon coupling to the different eigenmodes. Atomic units are used throughout the paper unless otherwise stated.

The modulus square of the autocorrelation function

$$A(t) = |\langle\alpha|\Psi(t)\rangle|^2 = \sum_{n,m} |c_n|^2|c_m|^2 \exp[-i(E_n - E_m)t] \tag{4}$$

with coefficients $|c_n|^2 = |M_{\alpha n}|^2|F_n|^2$ is formally equivalent to $P_{\alpha\to f}(t)$, the probability of going from a state $|\alpha\rangle$ to a state $|f\rangle$ in a pump-probe experiment involving two identical pulses with a time delay t. Therefore, Eq. (4) can be measured [1].

One of the salient features of Eq. (4) is that this time-dependent function shows revivals and partial revivals of the initial wave packet. Clearly not all of the infinitely many terms in Eq. (4) do contribute equally, since the pulse excitation covers only a finite energy interval of the spectrum $\{E_n\}$, see Eq. (1). Hence, our goal is to rewrite the double sum such that a systematic truncation to the most important terms is facilitated, yet retaining in the most accurate manner the different periodicities which give rise to the revival phenomena.

To reorder the contributions in the sum, we will make use of an expansion of the eigenenergies E_n around the mean excitation $E_{\overline{n}}$, which is well justified as long as the pulse excites a region of high density of states, so that the relative level spacing $(dE/dn|_{\overline{n}})/E_{\overline{n}} \ll 1$.

In a second step we will acknowledge the fact that for high frequency pulses the spectrum of highly charged ions is excited in a region of much lower density of states than in the traditional Rydberg regime.

A. Regrouping the sum

First we perform a Taylor expansion of the energy around the mean excitation energy $E_{\overline{n}}$, and split the expansion into two terms $\delta_n^\pm$ with even/odd powers of n, so that the energy differences become (see appendix A 1)

$$E_{\overline{n}+n} - E_{\overline{n}} \equiv \delta_n = \delta_n^+ + \delta_n^- \tag{5a}$$

where

$$\delta_n^+ = 2\pi \sum_{j=1}^{\infty} \frac{n^{2j}}{\bar{T}_{2j}}, \quad \delta_n^- = 2\pi \sum_{j=1}^{\infty} \frac{n^{2j-1}}{\bar{T}_{2j-1}} \tag{5b}$$

and

$$\frac{1}{\bar{T}_j} = \frac{1}{2\pi}\frac{1}{j!}\left|\frac{d^j E_{n+\overline{n}}}{dn^j}\right|_{n=0}. \tag{5c}$$

For the regrouping we assume that the dipole matrix elements $M_{\alpha\nu}$ do not vary much in the relevant terms of Eq. (4) and are therefore irrelevant for the summation. Moreover, the diagonal parts $m = n$ will only contribute a non-oscillating background, so that the time-dependent part of Eq. (4) simplifies to

$$a(t) = \sum_{n\neq m} W_{mn} \exp[-i(\delta_m - \delta_n)t], \tag{6}$$

with weights

$$W_{mn} = \exp[-(\delta_m^2 + \delta_n^2)/\sigma^2] \tag{7}$$

decreasing rapidly with increasing distance $\delta_{|n|}$ from the central energy. Here $\sigma = \sqrt{4\log 2}/T$ is the pulse width in frequency domain, see Eq. (1). The idea is now to arrange the double sum Eq. (6) into groups of terms which have similar Gaussian weight W_{nm}, where we order the weight according to $\delta_m \propto |m|$. From a basic element W_{nm} a quadruple of elements is generated by the two symmetry operations and their concatenation: exchange of the indices $(n, m) \to (m, n)$ (which amounts to complex conjugation), and point inversion $(n, m) \to (-n, -m)$. Note that m, n can be negative due to the shift of the indices by the value $\overline{n}$. Hence we may rewrite Eq. (6) as

$$\frac{a(t)}{2} = \sum_{0\leq n<m} W_{mn}\cos[(\delta_m - \delta_n)t] + W_{-m-n}\cos[(\delta_{-m} - \delta_{-n})t] \tag{8}$$

Making use of the symmetry properties of the δ_n from Eq. (5a), we get (see appendix A 2)

$$\frac{a(t)}{4} = \sum_{0\leq n<m} e^{-\frac{w_{mn}}{\sigma^2}} \left\{ C_{mn}\cos[(\delta_m^+ - \delta_n^+)t]\cos[(\delta_m^- - \delta_n^-)t] + S_{mn}\sin[(\delta_m^+ - \delta_n^+)t]\sin[(\delta_m^- - \delta_n^-)t] \right\}, \tag{9}$$

where

$$w_{mn} = (\delta_m^+)^2 + (\delta_m^-)^2 + (\delta_n^+)^2 + (\delta_n^-)^2 \tag{10a}$$

accounts for the even and odd exponents of the neighboring levels, and

$$\begin{aligned} C_{mn} &= \sum_{j=0}^{\infty} \frac{(\delta_m^+\delta_m^- + \delta_n^+\delta_n^-)^{2j}}{(2j)!\,\sigma^{4j}} 2^{2j} \\ S_{mn} &= \sum_{j=0}^{\infty} \frac{(\delta_m^+\delta_m^- + \delta_n^+\delta_n^-)^{2j+1}}{(2j+1)!\,\sigma^{4j+2}} 2^{2j+1} \end{aligned} \tag{10b}$$

are the coefficients of the cosine and sine terms in Eq. (9), respectively.

B. Expansion to lowest order around the mean energy

The final form of the autocorrelation function Eq. (9) is still an exact version of Eq. (6). While of little practical use, it reveals the structure quite well, which contains products of two trigonometric functions. Their meaning becomes obvious if we truncate the Taylor expansion Eq. (5a) around $E_{\overline{n}}$ to lowest order,

$$\delta_m^+ \simeq \frac{2\pi m^2}{\bar{T}_2}, \quad \delta_m^- \simeq \frac{2\pi m}{\bar{T}_1}. \tag{11}$$

Keeping only products of derivatives to second order, i.e., in times T_1^{-1}, T_2^{-1} and T_1^{-2}, reduces Eq. (9) to (see appendix A 3)

$$\begin{aligned} \frac{a_2(t)}{4} \quad &\simeq \sum_{0\leq n<m} e^{-\frac{4\pi^2\sigma_T^2}{T_1^2}(m^2+n^2)} \\ &\times \cos\left[2\pi(m^2-n^2)\frac{t}{\bar{T}_2}\right]\cos\left[2\pi(m-n)\frac{t}{\bar{T}_1}\right]. \end{aligned} \tag{12}$$

From this representation one can easily read off the standard essential periodicities in the autocorrelation function: the classical and revival periods. One can also directly see how periodic maxima of $a(t)$ turn into minima for certain time intervals, as we will show in the next section. However, as we will also see, a further simplification using the two energy values $E_{\overline{n}\pm1}$ next to the mean energy $E_{\overline{n}}$ can be made to construct the autocorrelation function $a_2(t)$. Notice that this is not an additional approximation: the phase in the cosine in Eq. (8), which is exact, is $(\delta_m - \delta_n)t = (E_{\overline{n}+m} - E_{\overline{n}+n})t$, so the discrete energy differences are the ones which determine the periodicity of the system.

C. Expansion to lowest order using finite differences in the energy eigenstates

The autocorrelation function in Eq. (9) contains energy derivatives (see Eq. (5c)). While they are usually taken as

continuous derivatives, we will consider finite differences

$$E'_{\overline{n}} \equiv \frac{(E_{\overline{n}+1} - E_{\overline{n}-1})}{2} = \frac{(\delta_1 - \delta_{-1})}{2} \qquad (13)$$
$$\frac{E''_{\overline{n}}}{2} \equiv \frac{(E_{\overline{n}+1} - 2E_{\overline{n}} + E_{\overline{n}-1})}{2} = \frac{(\delta_1 + \delta_{-1})}{2}$$

The motivation for this comes from the fact that for the X-ray excitation regime, the few states which contribute to the autocorrelation function (see table 1) are not necessarily narrowly spaced in energy, so that a Taylor expansion may not be very accurate.

On the other hand, using finite differences implies that one includes the most important terms in the autocorrelation function with *exact* phases. The most important pair is $(m, n) = (1, 0)$, since it gives rise to the terms with highest weights in the autocorrelation function, see Eq. (7). For this pair of indices, the phases in Eq. (12) become $E''_{\overline{n}}/2$ and $E'_{\overline{n}}$ (Eq. (13)). Therefore, these indices contribute to the autocorrelation function with the phases

$$2\cos\left[\frac{\delta_1 - \delta_{-1}}{2}t\right]\cos\left[\frac{\delta_1 + \delta_{-1}}{2}t\right] = \cos\left[(\delta_1 - \delta_0)t\right] + \cos\left[(\delta_{-1} - \delta_0)t\right], \qquad (14)$$

which are the phases of the two lowest order terms in Eq. (8) (note that $\delta_0 = 0$). The amplitude is slightly off due to truncating C_{mn} in Eq. (9) to the $j = 0$ contribution, see appendix A 3. However, this does not affect the periodicities of $a(t)$, which we will discuss next.

D. Difference of periodicities defined by continuous derivatives and finite differences

A natural question is how much the periods $\bar{T}_i$ defined by the continuous derivatives in Eq. (5a) differ from the periods T_i defined by finite differences. This can be best illustrated with an example, for which we take a hydrogenic Rydberg electron with spectrum $E_n = -Z^2/(2n^2)$ excited to $E_{\overline{n}}$. The standard definition for the classical period, understood as the orbiting period of a classical electron, is derived from the energy derivative

$$\bar{T}_c \equiv \bar{T}_1 = \frac{2\pi}{E'_{\overline{n}}} = \frac{2\pi\overline{n}^3}{Z^2}, \qquad (15)$$

while from finite differences we obtain

$$T_c \equiv T_1 = \frac{4\pi}{E_{\overline{n}+1} - E_{\overline{n}-1}} = \frac{2\pi(\overline{n}^2 - 1)^2}{\overline{n}Z^2}. \qquad (16)$$

The relative difference between both expressions is

$$\frac{\bar{T}_c - T_c}{\bar{T}_c} = \frac{2}{\overline{n}^2} - \frac{1}{\overline{n}^4}, \qquad (17)$$

which is noticeable for lower values of $\overline{n}$: it is around 1% for $\overline{n} = 14$ (with a relative level spacing $\Delta E_{\overline{n}}/E_{\overline{n}} = 2/\overline{n} = 0.3$), but less than 0.1% for $\overline{n} = 45$ (with $\Delta E_{\overline{n}}/E_{\overline{n}} = 0.07$). Similarly the revival times are

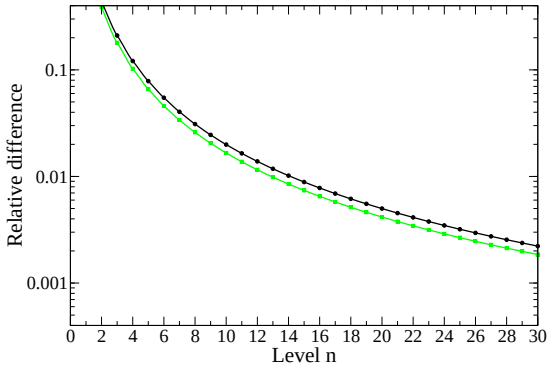

FIG. 2: (Color online) Relative differences between the standard approach (continuous derivatives) and our method, in logarithmic scale. Black line: classical period (Eq. (17)). Green line: revival time (Eq. (19)).

$$\bar{T}_r \equiv \bar{T}_2 = \frac{4\pi\overline{n}^4}{3Z^2}, \qquad (18)$$
$$T_r \equiv T_2 = \frac{4\pi\overline{n}^2(\overline{n}^2 - 1)^2}{Z^2(3\overline{n}^2 - 1)},$$

with a relative difference of

$$\frac{\bar{T}_r - T_r}{\bar{T}_r} = \frac{3}{\overline{n}^2} - \frac{4}{3\overline{n}^2 - 1}. \qquad (19)$$

This amounts to $\sim 0.85\%$ difference for $\overline{n} = 14$, and only 0.08% for $\overline{n} = 45$. Hence, both expressions merge for high quantum numbers, while for low quantum numbers with a larger spacing between energy levels a finite difference is a poor approximation to a derivative, see the sketch in Fig. 1. In our case, the energy differences are the "true" ones, so continuous derivatives are an approximation, which fails for low quantum numbers, as illustrated in Fig. 2. For this reason, we will use in the following the T_i derived from finite energy differences instead of the $\bar{T}_i$.

III. FOUR ESSENTIAL PERIODICITIES OF THE AUTOCORRELATION FUNCTION

A. Classical period and revival time

The autocorrelation function Eq. (9) or its truncation Eq. (12) reveal directly the classical period $T_c \equiv T_1$, for whose multiples the second cosine factor in each term becomes maximal. These are the two fundamental time scales emerging from the first and second order energy differences of energy levels next to the centrally excited one, as shown above.

A representative autocorrelation function for a radial Rydberg wave packet which exhibits these well known

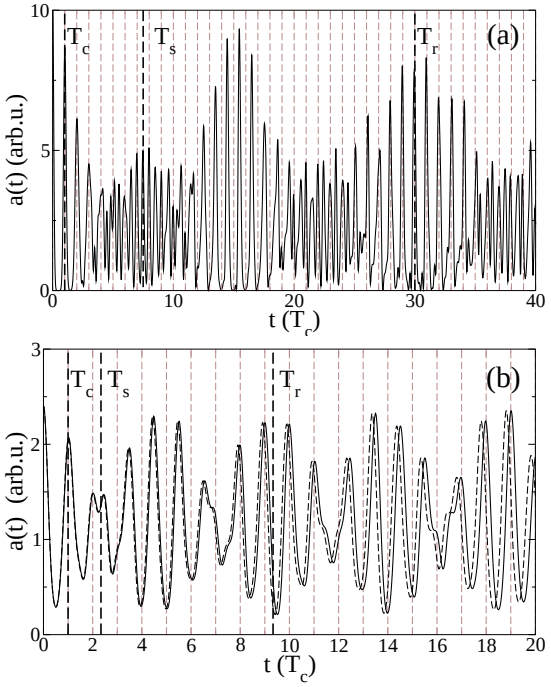

FIG. 3: Autocorrelation function for (a) $Z = 1$, $\overline{n} = 45$, FWHM=2 ps, and (b) $Z = 8$, $\overline{n} = 14$, FWHM=2 fs. Full lines: versus T_c. Dashed lines: versus $\bar{T}_c$. In (a) both are indistinguishable. The classical period T_c, revival time T_r, and the time for sign change T_s are shown with vertical lines.

features is shown in Fig. 3, for the high- and low-$\overline{n}$ regimes. The classical and revival times are indicated. Note that results for periods T_i and $\bar{T}_i$ coincide to the accuracy of the figure in the high-$\overline{n}$ case (Fig. 3a), while a discrepancy is visible in the low-$\overline{n}$ case of Fig. 3b.

B. The time T_s of sign change

At first glance, the wave packet in Fig. 3a shows a revival at $T_r/2$, but a closer inspection reveals that this is not an exact copy of the wave packet, since its maxima are shifted by half a period T_c (in between the vertical dashed lines). The revival at T_r is complete, with maxima close to full periods of T_c. Although noticed before [13, 25], there has been no formulation of the autocorrelation function which would reveal the shift directly. This is achieved in Eq. (6) with the products of two trigonometric functions and the cosine product dominating as revealed by Eq. (9). The first cosine function with its slow period T_r can be interpreted as an envelope to the rapidly oscillating second one with period T_c. Hence, we identify a time for sign change $T_s \equiv T_r/4$ at which the sign of the envelope changes, turning the maxima of the second cosine function into minima. This is the origin of the apparent shift in the position of the maxima.

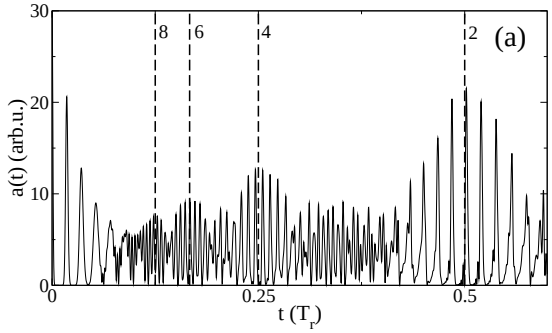

FIG. 4: Autocorrelation function for a Rydberg wave packet with $\overline{n} = 85$ and a pulse of 8 ps (a), The different fractional revivals are shown with vertical lines.

C. Partial revivals

As it is well known, in addition to the revivals, there appear fractional revivals at times

$$t = \frac{pT_r}{2(m^2 - n^2)}, \tag{20}$$

where the phase of the first cosine in Eq. (12) is a multiple of π. However, as the values of n, m increase, the corresponding Gaussian weights decrease. Therefore, the higher the order of the fractional revival, the lower its intensity. An example is shown in Fig. 4. Following the philosophy of keeping only the largest contribution, one can directly see from Eq. (12) how the partial revivals emerge by truncating the sum according to the dominant contributions of the Gaussian weights.

From Table II we expect that the largest contributions will arise from the fundamental pair $(n, m) = (1, 0)$, which leads to the fractional revival at $T_r/2$. The second largest contribution comes from the $(n, m) = (2, 0)$ term, which has an exponent of $n^2 + m^2 = 4$. According to Eq. (20) this contribution (with $p = 1$) should give rise to a fractional revival at $T_r/8$. If the third largest term, the pair $(n, m) = (2, 1)$ with an exponent of 5 is included, a new partial revival will appear as expected at $T_r/6$, although with a very small weight. This evolution can be seen in Fig. 5 for $Z = 1$, $\overline{n} = 85$ and FWHM = 8 ps. In Fig. 5a, the autocorrelation function emerges as more terms are added. The exact analytical value is shown in the top (thick black line). The periodicities due to the different terms of the sum are shown in Fig. 5b.

Overall, as can be seen from Eq. (12), two factors determine the maximum order of fractional revivals resolved in the autocorrelation function: the width of the pulse σ_T and the energy difference between the states adjacent to $\overline{n}$, as well as the inverse (discrete) classical revival time T_c in the combination σ_T/T_c: The shorter the pulse (small σ_T) and the smaller the energy differences (large T_c) the higher are these weights, and therefore more fractional revivals will appear in these cases.

Higher values of $\overline{n}$ with many states involved will create higher orders of fractional revivals, as shown in Fig. 4(a)

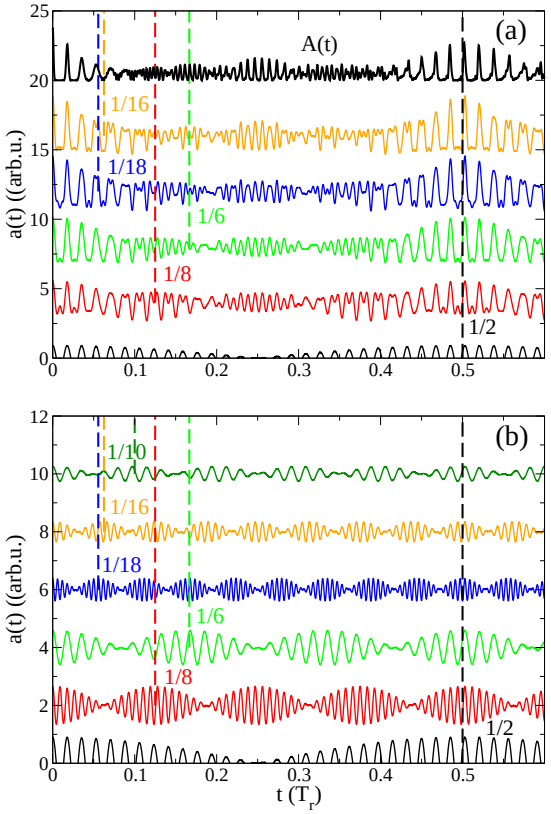

FIG. 5: (Color online) (a) Different truncations of the sum in Eq. (12), for $Z = 1$, $\overline{n} = 85$ and FWHM = 8 ps, including up to $(n, m) = (1, 0)$ (black), $(2, 0)$ (red), $(2, 1)$ (green), $(3, 0)$ (blue) and $(3, 1)$ (orange). The exact analytical value A(t) (Eq. (4)) is shown for comparison at the top of the upper figure (thick black). The expected position of the fractional revivals is shown with vertical lines (see text). In (b), the different components are shown separately (without summation) for the same cases plus for the pair $(3, 2)$ (in dark green).

TABLE II: Exponents m^2+n^2 for the approximate weights in Eq. (12) of contributions (m, n) giving rise to partial revivals $T_r/(m^2 - n^2)$, see Eq. (20).

pair (m,n)	exponent m^2+n^2	revival divisor (m^2-n^2)
(1,0)	1	1
(2,0)	4	4
(2,1)	5	3
(3,0)	9	9
(3,1)	10	8
(3,2)	13	5

for a Rydberg wave packet with roughly 13 participating states (see table 1) with $Z = 1$, $\overline{n} = 85$ and FWHM=8 ps.

IV. WAVEPACKET DYNAMICS IN THE LOW EXCITATION DOMAIN

We will now explicitly discuss the new regime of low quantum number wave packet dynamics. As sketched in Fig. 1b, for the case of a highly charged ion, i.e. with an effective atomic number $Z = 8$ (Fig. 1b), when the $\overline{n} = 14$ level is hit with a pulse of width FWHM=2 fs, only $k \sim 4$ levels are excited and the relative energy difference between the levels is large, thus one would expect periodicities obtained from a Taylor expansion to be less accurate.

The corresponding autocorrelation function (Eq. (4)) is shown in Fig. 3b, both against T_c (full lines), and against $\bar{T}_c$ (dashed lines). The discrepancy is clear and becomes already seizable around the first revival, for which $\bar{T}_c$ describes very poorly the periodicity and T_c remains almost exact. Also prominently visible are the maxima located at half-integer multiples of T_c around $T_r/2$ and at integer multiples of T_c close to the revival time T_r, as explained in Section III B.

The extreme case of a very low quantum number in the final state is shown in detail in Fig. 6. Here we consider a hydrogenic atom with an effective $Z = 12$ excited to $\overline{n} = 7$, with an ultrashort pulse of 0.1 fs with only 4 states participating, a situation which one may also consider as a multi-quantum beat phenomenon. The X-ray photon energy required for a $1s \to 7p$ transition in this system is $\omega = 1.92$ keV (we neglect the quantum defect). While the sign change of the extrema at $T_r/4$ is very clearly visible, revivals can no longer be identified. Also, the classical time $\bar{T}_c$ from a continuous energy derivative completely fails to predict the time scale (and therefore the position of the extrema) correctly after about 2 fs.

In Fig. 7b we see that the particular value of the dipole elements M_{in} has a small influence on the autocorrelation spectrum in this regime. In this figure, the same autocorrelation function as in (a) is shown (black line) with all dipole elements $M_{in} = 1$, together with the realistic calculation for $M_{in} = (2/n)^{3/2}$ (green line) [26]. The details of $a(t)$ vary, but the position of the peaks remains overall the same.

V. NON-RESONANT EXCITATIONS AND QUANTUM DEFECTS

In a general excitation process, the photon energy may not be resonant with any particular electronic transition. In this case

$$E_1 + \Omega \to E_{\overline{n}} + \epsilon. \tag{21}$$

We can identify this with an effective energy $E_{\overline{n}+\Delta n}$, where $0 < \Delta n < 1$. As Δn grows, the central energy goes from $E_{\overline{n}}$ to $E_{\overline{n}+1}$, and the classical period evolves approximately with the third power of $\overline{n} + \Delta n$ (see Eq. (16)). Notice that what really happens is that while the pairs of eigenvalues involved in the different beatings remain the

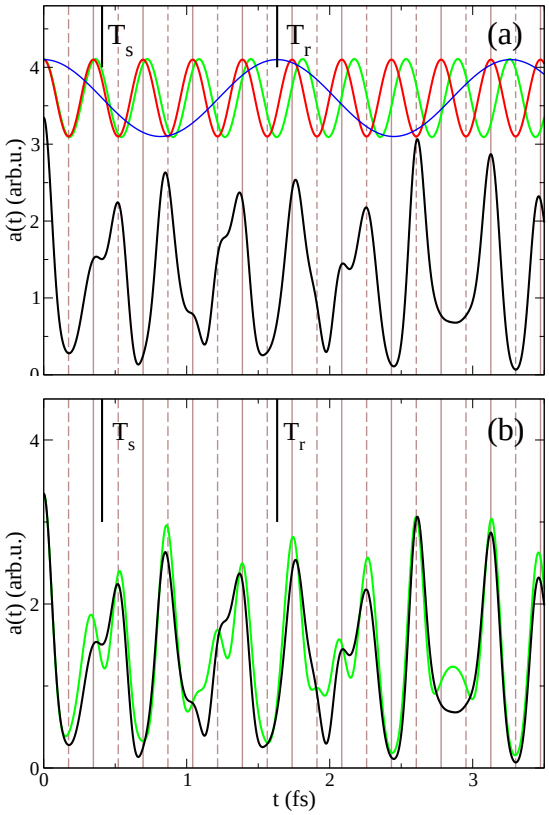

FIG. 6: (Color online) Autocorrelation function for $Z = 12$, $\overline{n} = 7$, FWHM=0.1 fs. (a) Black line: $a(t)$. Red line: $\cos(2\pi t/T_c)$. Green line: $\cos(2\pi t/\bar{T}_c)$. Blue line: $\cos(2\pi t/T_r)$. The vertical lines are multiples (full lines) and half-multiples (dashed lines) of T_c. (b) Same function compared with the case of varying dipole matrix elements M_{1n}, see text (green line).

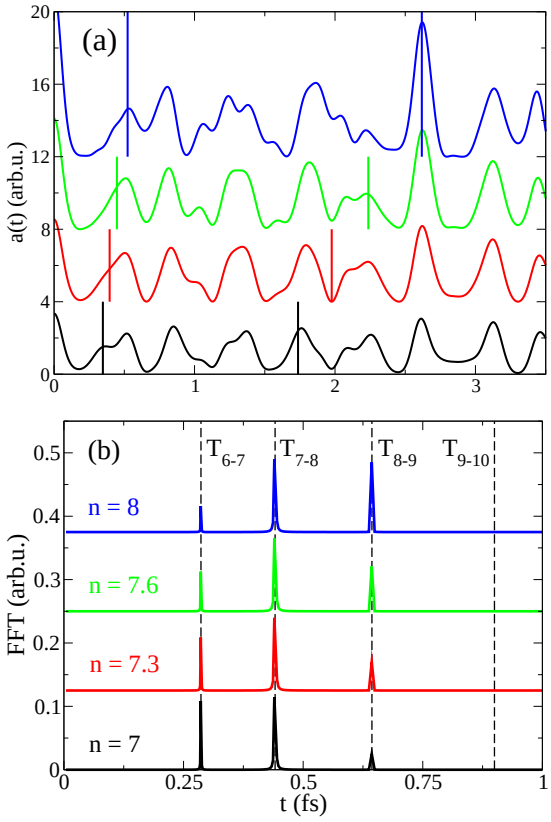

FIG. 7: (Color online) (a) Same as in Fig. 6, but for four photon energies, corresponding to effective values $\overline{n} = 7$, 7.3, 7.6 and 8. The values of T_c and $5T_c$ are drawn in each case with vertical lines. (b) Fourier transform of the cases in (a), using the two first terms in Eq. (12). Abscissas are expressed in terms of time as $t = 2\pi/\omega$. Vertical lines show the different periodicities, see text.

same, the relative weights in Eq. (1) are changing, and so is T_c. This is illustrated again for $Z = 12$ and FWHM = 0.1 fs in Fig. 7, for four different photon energies: 1.919 keV ($1s \rightarrow 7p$ transition), 1.922 keV ($\overline{n}$=7.3), 1.925 keV ($\overline{n}$=7.6) and 1.929 keV ($\overline{n}$=8). The autocorrelation function and the Fourier transform are shown for the four cases in (a) and (b), respectively. In the latter case, only two terms in Eq. (12) are used for simplicity, and abscissas are shown as a function of time. Vertical lines indicate the different periods, for $T_{a-b} = 2\pi/(E_a - E_b)$. While $\overline{n} = 7$ and 8 show only two relevant contributions, more terms appear in the spectrum at non-integer values of $\overline{n}$.

We have explored so far the hydrogenic case in which only one electron is bound to a nucleus of charge Z. However, if the system contains more than one electron, we might consider a nucleus of charge $Z + p$ and p core electrons. The wave packet is then subject to an effective potential with a Coulombic tail of charge Z, whose eigenenergies are given by

$$E_n^\alpha = -\frac{Z^2}{2n_\alpha^2}, \tag{22}$$

where $n_\alpha = n - \alpha$. The quantum defect α depends on the angular momentum, but is almost independent on the quantum number n for $n \gg 1$. The shift in the energies affects the periodicities of the system [27, 28]: With the period for the hydrogenic case ($\alpha = 0$) and the multi-electron case ($\alpha \neq 0$) denoted by T_c and T_c^α, respectively, the relative shift due to the quantum defect α is given by

$$\begin{aligned} s_{\overline{n}}(\alpha) &= \frac{T_c^\alpha - T_c}{T_c} = \frac{(\overline{n}_\alpha^2 - 1)^2}{(\overline{n}^2 - 1)^2}\frac{\overline{n}}{\overline{n}_\alpha} - 1 \\ &= \alpha\left[\frac{1 + \overline{n}_\alpha \overline{n}(2 - \alpha^2 + 3\alpha\overline{n} - 3\overline{n}^2)}{\overline{n}_\alpha(\overline{n}^2 - 1)^2}\right]. \end{aligned} \tag{23}$$

This shift accumulates in time and should assume the value

$$\frac{T_r}{T_c} s_{\overline{n}}(\alpha) = \frac{2\overline{n}^3}{3\overline{n}^2 - 1} s_{\overline{n}}(\alpha) \sim -2\alpha \tag{24}$$

around T_r. This prediction is valid even in the low $\overline{n}$ regime, as is shown in Fig. 8 for $Z = 8$, $\overline{n} = 9$ and a pulse length of 0.4 fs, using both, $\alpha = 0$ and 0.3.

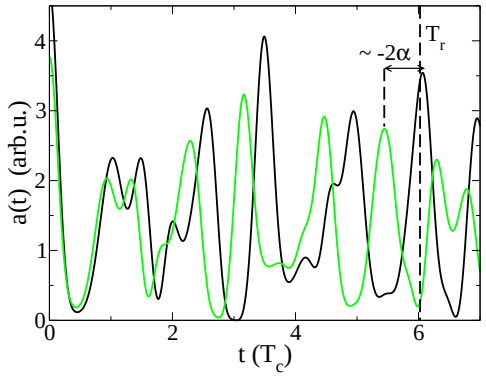

FIG. 8: (Color online) Effect of the quantum defect on the autocorrelation function, for $Z = 8$, $\overline{n} = 9$ and FWHM = 0.4 fs, using $\alpha = 0$ (black) and $\alpha = 0.3$ (green). Time is plotted in units of T_c, the classical period for the case with $\alpha = 0$. The shift in the peaks around T_r is $\sim -2\alpha$.

VI. CONCLUSIONS

We have explored the dynamics of electron wave packets in the new regime of low atomic excitation which can be realized by short and intense laser pulses of high photon energy, e.g., from XFEL light sources. We have shown that the standard analysis of wave packet dynamics with characteristic periodicities carries over to the low excitation regime, but only when the periods are calculated from differences of the two energy levels bracketing the main excitation level $\overline{n}$ instead of using continuous derivatives. Moreover, we have formulated the autocorrelation function in such a way that a new time scale appears as an important structural element, namely a quarter of the revival time $T_s = T_r/4$, where the sign of the extrema in the autocorrelation function flip sign. This is a prominent feature in low excitation wave packets and explains the "shift" in the maxima noticed previously in the high $\overline{n}$ domain. Hence, the analytical and numerical tools are now available to analyze experiments on wave packet dynamics with intense short light pulses of high frequency.

JMR acknowledges support in part by the National Science Foundation under Grant No. NSF PHY05-51164 during a visit of KITP at the University of Santa Barbara. PR acknowledges support in part from the MICINN projects FIS2010-15127 and JCI2009-03793, and the COST action CM0702.

Appendix A: Regrouping the sum in the autocorrelation function

1. Terms in the Taylor expansion

The spectrum can be expanded around $E_{\overline{n}}$:

$$E_{n+\overline{n}} - E_{\overline{n}} \equiv \delta_n = \delta_n^+ + \delta_n^- \tag{A1}$$

The Taylor expansion is

$$\begin{aligned} E_m - E_{n_0} &\sim \sum_{j=1}^{\infty} \frac{1}{j!} \frac{d^j E_m}{dm^j}\Big|_{m=n_0} (m-n_0)^j \\ &= \sum_{j=1}^{\infty} \frac{1}{(2j-1)!} \frac{d^{2j-1} E_m}{dm^{2j-1}}\Big|_{m=n_0} (m-n_0)^{2j-1} \\ &\quad + \sum_{j=1}^{\infty} \frac{1}{(2j)!} \frac{d^{2j} E_m}{dm^{2j}}\Big|_{m=n_0} (m-n_0)^{2j} \end{aligned} \tag{A2}$$

At $m = n + n_0$ it is

$$\begin{aligned} E_{n+n_0} - E_{n_0} &\sim \sum_{j=1}^{\infty} \frac{1}{(2j-1)!} \frac{d^{2j-1} E_{n+n_0}}{dn^{2j-1}}\Big|_{n=0} n^{2j-1} \\ &\quad + \sum_{j=1}^{\infty} \frac{1}{(2j)!} \frac{d^{2j} E_{n+n_0}}{dn^{2j}}\Big|_{n=0} n^{2j}, \end{aligned} \tag{A3}$$

so if we define

$$\frac{1}{\bar{T}_j} \equiv \frac{1}{2\pi j!} \frac{d^j E_{n+n_0}}{dn^j}\Big|_{n=0}, \tag{A4}$$

then

$$\begin{aligned} E_{n+n_0} - E_{n_0} &\sim 2\pi \sum_{j=1}^{\infty} \frac{n^{2j-1}}{\bar{T}_{2j-1}} + 2\pi \sum_{j=1}^{\infty} \frac{n^{2j}}{\bar{T}_{2j}} \\ &\equiv \delta_n^- + \delta_n^+. \end{aligned} \tag{A5}$$

2. Final expression for $a(t)$

An expansion of the cosines in Eq. (8) brings

$$\begin{aligned} a(t)/2 &= \sum_{0 \le n < m} W_{mn} \Big[\cos[(\delta_m^+ - \delta_n^+)t] \cos[(\delta_m^- - \delta_n^-)t] \\ &\quad - \sin[(\delta_m^+ - \delta_n^+)t] \sin[(\delta_m^- - \delta_n^-)t] \Big] \\ &\quad + W_{-m-n} \Big[\cos[(\delta_{-m}^+ - \delta_{-n}^+)t] \cos[(\delta_{-m}^- - \delta_{-n}^-)t] \\ &\quad - \sin[(\delta_{-m}^+ - \delta_{-n}^+)t] \sin[(\delta_{-m}^- - \delta_{-n}^-)t] \Big]. \end{aligned} \tag{A6}$$

Due to the symmetric properties of the energy differences, it is $\delta_{-n}^+ = \delta_n^+$ and $\delta_{-n}^- = -\delta_n^-$, so

$$\delta_{-m}^+ - \delta_{-n}^+ = \delta_m^+ - \delta_n^+, \tag{A7}$$

$$\delta_{-m}^- - \delta_{-n}^- = -(\delta_m^- - \delta_n^-). \tag{A8}$$

The coefficients are

$$W_{nm} = e^{-\left[(\delta_m^2 + \delta_n^2)/\sigma^2\right]} = e^{-w_{mn}/\sigma^2} e^{-2v_{mn}/\sigma^2}, \tag{A9}$$

where w_{mn} is defined in Eq. (10a), and

$$v_{mn} \equiv \delta_m^+ \delta_m^- + \delta_n^+ \delta_n^-. \tag{A10}$$

Again due to symmetry reasons, $w_{-m-n} = w_{mn}$ and $v_{-m-n} = -v_{mn}$, and thus

$$W_{-n-m} = e^{-w_{mn}/\sigma^2} e^{2v_{mn}/\sigma^2}. \quad \text{(A11)}$$

With this, Eq. (A6) becomes

$$\begin{aligned} a(t)/2 \;=\; & \sum_{0\le n<m} W_{mn}\Big[\cos[(\delta_m^+ - \delta_n^+)t]\cos[(\delta_m^- - \delta_n^-)t] \\ & - \sin[(\delta_m^+ - \delta_n^+)t]\sin[(\delta_m^- - \delta_n^-)t]\Big] \\ & + W_{-m-n}\Big[\cos[(\delta_m^+ - \delta_n^+)t]\cos[(\delta_m^- - \delta_n^-)t] \\ & + \sin[(\delta_m^+ - \delta_n^+)t]\sin[(\delta_m^- - \delta_n^-)t]\Big]. \quad \text{(A12)} \end{aligned}$$

The terms with cosines gather in a term with coefficient

$$\begin{aligned} W_{mn} + W_{-m-n} \;&=\; e^{-w_{mn}/\sigma^2}\left(e^{-2v_{mn}/\sigma^2} + e^{2v_{mn}/\sigma^2}\right) \\ &=\; 2e^{-w_{mn}/\sigma^2}\cosh\left[\frac{2v_{mn}}{\sigma^2}\right], \quad \text{(A13)} \end{aligned}$$

while the terms with sines gather with a coefficient

$$\begin{aligned} -W_{mn} + W_{-m-n} \;&=\; e^{-w_{mn}/\sigma^2}\left(-e^{-2v_{mn}/\sigma^2} + e^{2v_{mn}/\sigma^2}\right) \\ &=\; 2e^{-w_{mn}/\sigma^2}\sinh\left[\frac{2v_{mn}}{\sigma^2}\right]. \quad \text{(A14)} \end{aligned}$$

Therefore,

$$(W_{mn} + W_{-m-n})e^{w_{mn}/\sigma^2} = 2\sum_{j=0}^{\infty}\frac{(2v_{mn})^{2j}}{(2j)!\sigma^{4j}}, \quad \text{(A15)}$$

and

$$(-W_{mn} + W_{-m-n})e^{w_{mn}/\sigma^2} = 2\sum_{j=0}^{\infty}\frac{(2v_{mn})^{2j+1}}{(2j+1)!\sigma^{4j+2}}, \quad \text{(A16)}$$

which are respectively $2C_{mn}$ and $2S_{mn}$, as defined in Eq. (10a). This way we obtain Eq. (9):

$$\begin{aligned} a(t)/4 \;=\; & \sum_{0\le n<m} e^{-\frac{w_{mn}}{\sigma^2}}\Big[C_{mn}\cos[(\delta_m^+ - \delta_n^+)t]\cos[(\delta_m^- - \delta_n^-)t] \\ & + S_{mn}\sin[(\delta_m^+ - \delta_n^+)t]\sin[(\delta_m^- - \delta_n^-)t]\Big]. \quad \text{(A17)} \end{aligned}$$

3. Lowest order of the expansion

If we take the lowest order ($j = 1$) in the definition of δ_m^+ and δ_m^- at Eq. (11), then

$$\begin{aligned} \delta_m^+ - \delta_n^+ \;&=\; \frac{2\pi}{\bar{T}_2}(m^2 - n^2), \\ \delta_m^- - \delta_n^- \;&=\; \frac{2\pi}{\bar{T}_1}(m - n), \quad \text{(A18)} \end{aligned}$$

and

$$\begin{aligned} w_{mn} \;&=\; (\delta_m^+)^2 + (\delta_m^-)^2 + (\delta_n^+)^2 + (\delta_n^-)^2 \\ &=\; 4\pi^2\left(\frac{m^4}{\bar{T}_2^2} + \frac{m^2}{\bar{T}_1^2} + \frac{n^4}{\bar{T}_2^2} + \frac{n^2}{\bar{T}_1^2}\right), \quad \text{(A19)} \end{aligned}$$

which at second order in the derivatives is

$$w_{mn} \;\sim\; \frac{4\pi^2}{\bar{T}_1^2}(m^2 + n^2). \quad \text{(A20)}$$

The lowest order of the sums in C_{mn} and S_{mn} is $j = 0$, so

$$\begin{aligned} C_{mn} \;&=\; 1, \\ S_{mn} \;&=\; \frac{2v_{mn}}{\sigma^2}. \quad \text{(A21)} \end{aligned}$$

Since $S_{mn} = 0$ at second order in the derivatives, and using $\sigma_T = 1/\sigma$, we obtain Eq. (12),

$$\begin{aligned} a_2(t)/4 \sim \sum_{0\le n<m} & e^{-\frac{4\pi^2\sigma_T^2}{\bar{T}_1^2}(m^2+n^2)}\cos\left[2\pi(m^2 - n^2)\frac{t}{\bar{T}_2}\right] \\ & \times \cos\left[2\pi(m - n)\frac{t}{\bar{T}_1}\right]. \quad \text{(A22)} \end{aligned}$$

[1] G. Alber, H. Ritsch, P. Zoller, *Phys. Rev. A* **34**, 1058 (1986)

[2] J. Parker, C. R. Stroud, Jr., *Phys. Rev. Lett.* **56**, 716 (1986).

[3] F. Grossmann, J. M. Rost and W. P. Schleich, *J. Phys. A* **30**, L277 (1997).

[4] T. Ergler, A. Rudenko, B. Feuerstein, K. Zrost, C. D. Schröter, R. Moshammer, J. Ullrich, *Phys. Rev. Lett.* **97**, 193001 (2006).

[5] S. De, I. A. Bocharova, M. Magrakvelidze, D. Ray, W. Cao, B. Bergues, U. Thumm, M. F. Kling, I. V. Litvinyuk and C. L. Cocke, *Phys. Rev. A* **82**, 013408 (2010)

[6] C. R. Calvert,. W. A. Bryan, W. R. Newell and I. D. Williams, *Phys. Reports* **491**, 1 (2010)

[7] H. Katsuki, H. Chiba, C. Meier, B. Girard and K. Ohmori *Phys. Chem. Chem. Phys.*, **12**, 5189 (2010)

[8] J. Keeling and V. Gurarie, *Phys. Rev. Lett.* **101**, 033001 (2008)

[9] V. Krueckl and T. Kramer, *New J. Phys* **11**, 093010 (2009).

[10] C. Leichtle, I. Sh. Averbukh and W. P. Schleich, *Phys. Rev. A* **54**, 5299 (1996)

[11] D. L. Aronstein and C. R. Stroud, Jr., *Laser Phys.* **15**, 1496 (2005)

[12] R. W. Robinett, *Phys. Rep.* **392**, 1-119 (2004)

[13] I. Sh. Averbukh and N. F. Perelman, *Phys. Lett. A* **139**, 449 (1989)

[14] R. Veilande and I. Bersons, *J. Phys. B* **40**, 2111 (2007)

[15] J. A. Yeazell and C. R. Stroud Jr., *Phys. Rev. A* **43**, 5153 (1991).

[16] G. Della Valle, M. Savoini, M. Ornigotti, P. Laporta, V. Foglietti, M. Finazzi, L. Duò and S. Longhi, *Phys. Rev. Lett.* **102**, 180402 (2009).

[17] S. Ghosh and J. Banerji, *J. Phys. B* **40**, 3545 (2007)

[18] A. Schubert, K. Renziehausen and V. Engel, *Phys. Rev. A* **82**, 013419 (2010)

[19] Merkel, W., Averbukh, I. Sh., Girard, B., Paulus, G. G., Schleich, W. P., *Fortschr. Phys.* **54**, 856 (2006).

[20] E. Romera and F. de los Santos, *Phys. Rev. Lett.* **99**, 263601 (2007).

[21] V. Ayvazyan et al., *Eur. J. Phys. D* **37**, 297 (2005).

[22] S. Knoop, M. Keim, H. J. Ludde, T. Kirchner, R. Morgenstern, R. Hoekstra, *J. Phys. B* **38**, 3163 (2005).

[23] D Fischer, B Feuerstein, R D DuBois, R Moshammer, J R Crespo López-Urrutia, I Draganic, H Lorch, A N Perumal and J Ullrich, *J. Phys. B* **35**, 1369 (2002).

[24] V. Averbukh, U. Saalmann and J. M. Rost, *Phys. Rev. Lett.* **104**, 233002 (2010).

[25] J. A. Yeazell, M. Mallalieu and C. R. Stroud Jr., *Phys. Rev. Lett.* **64**, 2007 (1990)

[26] N. B. Delone, S. P. Goreslavsky and Krainov, V. P., *J. Phys. B* **27**, 4403 (1994)

[27] R. Bluhm, V. A. Kostelecký, *Phys. Rev. A* **50**, R4445 (1994).

[28] J. Wals, H. H. Fielding and H. B. van Linden van der Heuvell, *Physica Scripta* **T58**, 62 (1995).